

# Holonomic quantum computation with all resonant control in circuit QED

Zheng-Yuan Xue,<sup>1,\*</sup> Jian Zhou,<sup>2,1,3,†</sup> and Yong Hu<sup>4,‡</sup>

<sup>1</sup>*Guangdong Provincial Key Laboratory of Quantum Engineering and Quantum Materials, and School of Physics and Telecommunication Engineering, South China Normal University, Guangzhou 510006, China*

<sup>2</sup>*Department of Electronic Communication Engineering, Anhui Xinhua University, Hefei, 230088, China*

<sup>3</sup>*National Laboratory of Solid State Microstructure, Nanjing University, Nanjing 210093, China*

<sup>4</sup>*School of Physics, Huazhong University of Science and Technology, Wuhan 430074, China*

(Dated: December 3, 2024)

The implementation of holonomic quantum computation generally requires controllable and complicated interaction among addressable multi-level systems, which is challenging on superconducting circuit. Here, we propose a scalable architecture for non-adiabatic holonomic quantum computation on a circuit QED lattice with hybrid transmon and photon encoding of the logical qubits in a decoherence-free subspace. With proper driven on the transmon, we can obtain tunable resonate interaction between the transmon and each of the resonators, which leads to arbitrary single-qubit operation on the encoded logical qubit. Meanwhile, for a nontrivial two-qubit gate, we only need resonate interactions among the three resonators from the two logical qubits, which can be induced by commonly coupled to a grounding SQUID with ac magnetic driven. More importantly, our scheme is achieved with all resonate interactions among the involved elements, and thus leads to quantum gates with very high fidelity. Therefore, our scheme opens up the possibility of realizing high fidelity universal holonomic quantum computation in solid-state system.

PACS numbers: 03.67.Lx, 42.50.Dv, 85.25.Cp

The implementation of quantum computation requires a scalable quantum system that can support a universal set of quantum gates. As quantum dynamics will generally be influenced by the decoherence effect, the fidelity of a quantum gate will be limited by it. It is well known that geometric phases [1, 2] and holonomies [3, 4] from cyclical evolutions of quantum systems depend only on global geometric properties of the evolution paths, and thus are largely insensitive to some local noises. Therefore, holonomic quantum computation (HQC), quantum computation based on non-abelian quantum holonomies, has emerged as a promising way of robust quantum computation [5–11]. However, adiabatic geometric phases require the involved quantum paths should be traveled under the adiabatic condition, and thus the time needed for the evolution maybe on the same order of the coherence time of the used qubits in typical quantum systems [12, 13]. Therefore, many renewed efforts have recently been given in consulting quantum gates based on non-adiabatic evolution both theoretically and experimentally [14–25].

However, the implementation of universal HQC on superconducting circuits is very difficult. For the implementation of HQC, one generally needs controllable and complicated interaction among addressable multi-level systems [7], at least three-level systems [14]. For superconducting circuits, it is well known that the anharmonicity of the energy spectrum is small, and thus limit the coupling strength between neighboring levels [16, 26]. Furthermore, the wanted complicated interaction is more challenging on superconducting circuits and the experiment in Ref. [16] only implemented single-qubit gates. Recently, we have proposed to implement universal HQC based on only two levels in the transmon qubits [24],

which solves partially the problem. But, the interaction needed for a nontrivial two-qubit gate is induced from dispersive qubit-cavity interaction, and thus limits the gate fidelity. Therefore, this appears to be a main obstacle for physical implementation of universal HQC on superconducting circuits.

Here, we propose a practical scheme for non-adiabatic HQC on a circuit QED lattice. In our scheme, we also incorporate the decoherence-free subspaces (DFS) [27–29] encoding of the logical qubits, which consists of both transmon and photon states, i.e., a logical qubit consists of two transmission line resonators (TLRs) commonly and dispersive coupled to a transmon qubit. With proper driven on the transmon, we can obtain tunable resonate interaction between the transmon and each of the resonators, which can be used to obtain arbitrary operation on the logical qubit. Meanwhile, for a nontrivial two logical qubit gate, we only need resonate interactions among the three TLRs from the two logical qubits, which can be induced by commonly coupled to a grounding SQUID with ac magnetic driven. That is to say, due to this exotic encoding, we can achieve universal HQC with all resonate interactions among the involved elements, and thus lead to quantum gates with very high fidelity. Therefore, our scheme opens up the possibility of realizing universal HQC in solid-state system.

We now start to present our scheme and the setup we considered is schematically illustrated in Fig. 1, which is a scalable coupled circuit QED lattice. The circles with different color denote the TLRs of different frequency and the square with cross inside denotes a transmon qubit. The dashed bonds denote photon hopping between neighbouring TLRs. A logical qubit is encoded in DFS by two

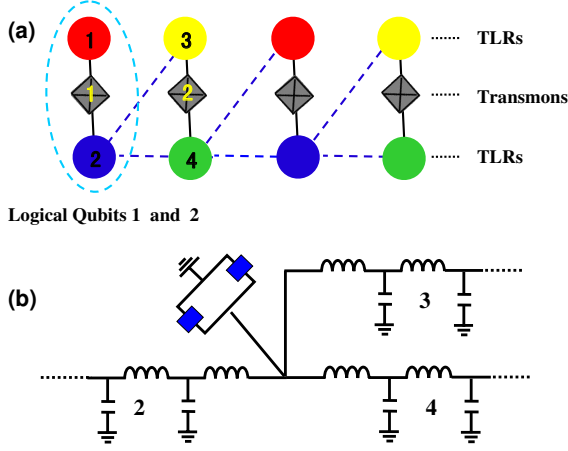


FIG. 1. (a) The proposed setup for our proposal. The circles with different color denote the TLRs of different frequency. The squares with crosses inside denote superconducting transmon qubits. The elements in the dashed ellipse is encoded as the first logical qubit. The dashed bonds denote the photon hopping between the selected TLRs, which are used for implementing two-qubit gates. (b) Example of the coupling configuration for a nontrivial two-qubit gate.

TLRs capacitively coupled to a transmon [30], as shown by the dashed ellipse in Fig. 1a. Then the interaction of the whole quantum system, in units of  $\hbar = 1$ , can be written as

$$H_S = \frac{\omega_q}{2} \sigma^z + \sum_{j=1}^2 \omega_{c,j} a_j^\dagger a_j + \sum_{j=1}^2 (g_j a_j \sigma^+ + \text{H.c.}), \quad (1)$$

where  $a_j^\dagger (a_j)$  is the creation (annihilation) operator of  $j$ th TLR with frequency  $\omega_{c,j}$ ,  $\omega_q$  is the frequency of the transmon qubit,  $\sigma^z$  is the Pauli matrix,  $g_j$  (assumed to be real) is the coupling strength between the qubit and  $j$ th TLR,  $\sigma^-$  and  $\sigma^+$  is the lower and upper operator of the transmon, respectively.

We consider the case of  $\Delta_j \gg g_j$  with  $\Delta_j = \omega_{c,j} - \omega_q$ . Then, the qubit-TLR interaction, represented by the last term of  $H_S$ , only acts perturbatively in this dispersive regime. To get resonant interaction between the selected TLR and the transmon qubit, the qubit is biased by an ac magnetic flux, which will introduce periodical modulation [31] of the qubit transition frequency in the form of

$$\omega_q(t) = \omega_q + \sum_{j=1}^2 \varepsilon_j \sin(\nu_j t - \phi_j). \quad (2)$$

As the transmon is placed in the middle of the two TLRs, we can drive the transmon by applying a well-controlled, two-tone microwave drive. For the presented experiments [30, 32], the transmon can tune to idle state transition frequency  $\omega_q$  with miniature superconducting coils mounted underneath the chip. This modulation may effectively

turn the qubit's sideband on resonance with the cavity frequency. To see this, we move to the rotating frame defined by

$$U = \exp \left[ \sum_{j=1}^2 i \sigma^z \frac{\alpha_j}{2} \cos(\nu_j t - \phi_j) - i \omega_{c,j} a_j^\dagger a_j t - i \frac{\omega_q}{2} \sigma^z t \right]$$

with  $\alpha_j = \varepsilon_j / \nu_j$ . Then, the transformed Hamiltonian reads

$$H'(t) = \left( g_1 a_1^\dagger \sigma^- e^{i\Delta_1 t} + g_2 a_2^\dagger \sigma^- e^{i\Delta_2 t} \right) \times \prod_{j=1}^2 \sum_{m=-\infty}^{\infty} i^m J_m(\alpha_j) e^{im(\nu_j t - \phi_j)} + \text{H.c.}, \quad (3)$$

where  $J_m(\alpha_j)$  being Bessel functions of the first kind. Under the condition of  $\nu_j = \Delta_j$ , the effective resonant interaction will be

$$H_{\text{eff}} = g [J_1(\alpha_1) a_1^\dagger \sigma^- + J_0(\alpha_1) a_2^\dagger \sigma^- e^{i\phi'} + \text{H.c.}], \quad (4)$$

where  $\phi' = \phi_2 - \phi_1$ , and  $g = g' J$  with  $g_1 = g_2 = g'$  and  $J_0(\alpha_2) = J_1(\alpha_2) = J$ , i.e.,  $\alpha_2 \simeq 1.4347$ . In this way, we have a full control over the coupling strength by varying the external driven ac magnetic flux, i.e., the amplitude  $\varepsilon_1$  and phase  $\phi_1$ . Moreover, we have applied the rotating wave approximation and the omitted terms has a smallest oscillating frequency of  $\Delta = |\Delta_2 - \Delta_1|$ , i.e.,

$$H'_1 = g \left[ J_1(\alpha_1) a_2^\dagger \sigma^- e^{i\Delta t} + J_0(\alpha_1) a_1^\dagger \sigma^- e^{-i\Delta t + \phi'} + \text{H.c.} \right]. \quad (5)$$

We now move to construct a universal set of non-adiabatic holonomic single-qubit quantum gate based on the Hamiltonian in Eq. (4). The DFS we considered here is

$$S_1 = \{|100\rangle, |001\rangle, |010\rangle\} \equiv |0\rangle_L, |1\rangle_L, |E\rangle_L,$$

where the subscript  $L$  denote the states belong to the logical qubit,  $|E\rangle_L$  the ancillary state and  $|100\rangle \equiv |1\rangle_1 \otimes |0\rangle_q \otimes |0\rangle_2$ , i.e., they denote the states of the first TLR, transmon and the second TLR, respectively. By this encoding, the Hamiltonian of the resonant quantum system consisting of two TLRs and a transmon reduces to

$$H_1 = \lambda_1 \left( \sin \frac{\theta}{2} e^{i\phi} |E\rangle_L \langle 0| - \cos \frac{\theta}{2} |E\rangle_L \langle 1| \right) + \text{H.c.}, \quad (6)$$

where  $\phi = \phi' + \pi$ , both  $\lambda_1 = g \sqrt{J_1^2(\alpha_1) + J_0^2(\alpha_1)}$  and  $\tan(\theta/2) = J_1(\alpha_1)/J_0(\alpha_1)$  can be tuned by  $\varepsilon_1$  from the driven field. In this case, a  $\Lambda$ -type Hamiltonian in the DFS is constructed with all resonant interaction, from which arbitrary single-qubit holonomic quantum gate can be obtained. In the dressed state representation, two lower states of this three-level system are

$$\begin{aligned} |d\rangle_L &= \cos \frac{\theta}{2} |0\rangle_L + \sin \frac{\theta}{2} e^{i\phi} |1\rangle_L, \\ |b\rangle_L &= \sin \frac{\theta}{2} e^{-i\phi} |0\rangle_L - \cos \frac{\theta}{2} |1\rangle_L. \end{aligned} \quad (7)$$

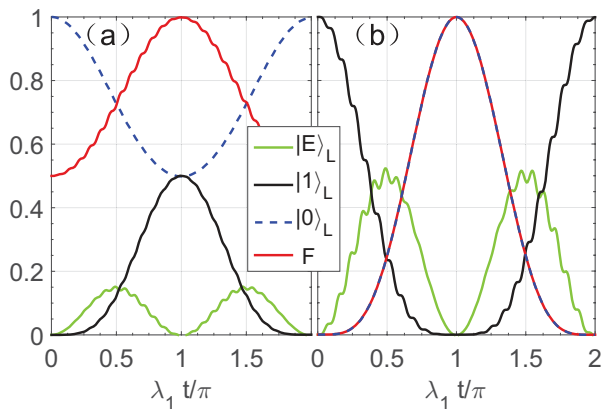


FIG. 2. Qubit states population and fidelity under single-qubit operator (a)  $U_1(\pi/4, 0)$  with initial state  $|0\rangle_L$  and (b)  $U_1(\pi/2, 0)$  with initial state  $|1\rangle_L$ .

It is obviously that the dark state  $|d\rangle_L$  decouples from the 'bright' state  $|b\rangle_L$  and the excited state  $|E\rangle_L$ , while the 'bright' state  $|b\rangle_L$  couples to the excited state  $|E\rangle_L$  with effective Rabi frequency  $\lambda_1$ . When the condition  $\lambda_1\tau_1 = \pi$  is satisfied, the dressed states undergo a cyclic evolution. Therefore, the time evolution operation will ensure the states evolving as  $|\psi_i(t)\rangle_L = U_1(t)|\psi_i(0)\rangle_L$ . Moreover, as  $\langle\psi_i(t)|H_1|\psi_i(t)\rangle = 0$ , there is no transition between the two time-dependent state, i.e., the evolution satisfies the parallel-transport condition. Therefore, the evolution operator  $U_1 = \exp(-i\int_0^{\tau_1} H_1 dt)$  can realize the holonomic operations under the above two conditions. In the space spanned by  $\{|0\rangle_L, |1\rangle_L\}$ ,

$$U_1 = \begin{pmatrix} \cos\theta & \sin\theta e^{-i\phi} \\ \sin\theta e^{i\phi} & -\cos\theta \end{pmatrix}, \quad (8)$$

where  $\theta$  and  $\phi$  can be chosen by tuning the amplitude and relative phase of driving laser beams, then a set of arbitrary single qubit operations can be achieved non-adiabatically.

Inevitably, the implementation will suffer from decoherence. Considering the main decoherence effect, the relaxation rate  $\gamma$ , dephasing rate  $\gamma_\phi$  of the transmon and the decay rate  $\kappa$  of the cavity, we can simulate the performance of the gates using the Lindblad master equation [33]

$$\begin{aligned} \dot{\rho} = & -i[H_1 + H'_1, \rho] + \frac{\kappa}{2}[\mathcal{L}(a_1) + \mathcal{L}(a_2)] \\ & + \frac{\gamma}{2}\mathcal{L}(\sigma^-) + \frac{\gamma_\phi}{2}\mathcal{L}(\sigma^z), \end{aligned} \quad (9)$$

where  $\rho$  is the density matrix of the considered system,  $\mathcal{L}(A) = 2A\rho A^\dagger - A^\dagger A\rho - \rho A^\dagger A$  is the Lindblad operator. We consider the Hadamard and NOT gates as two typical examples, which correspond to  $\theta = \pi/4$  and  $\pi/2$  with  $\phi = 0$ , respectively. To make the total coupling to be strong, we have used the following conservative set of experimental parameters. The energy splitting of

the transmon qubit and the frequencies of the two TLRs are chosen to be  $\omega_q = 2\pi \times 6$  GHz,  $\omega_{c,1} = 2\pi \times 6.5$  GHz,  $\omega_{c,2} = 2\pi \times 6.75$  GHz, respectively, which correspond to  $\Delta_1 = 2\pi \times 0.5$  GHz and  $\Delta_2 = 1.5\Delta_1$ . In this way, the intrinsic geometric coupling between the two TLRs due to the transmon can be neglected as the frequency difference is much larger [34]. For the Hadamard gate, we may modulate  $\alpha_1 = \varepsilon_1/\Delta_1 \simeq 0.7661$  so that  $J_0(\alpha_1) = 0.8585$  and  $J_1(\alpha_1) = 0.3556$ , which corresponds to  $J_1(\alpha_1)/J_0(\alpha_1) \simeq 0.4142 \simeq \tan(\theta/2)$ . Then, choosing  $g' = 2\pi \times 25$  MHz leads to  $\lambda_1 \simeq 2\pi \times 12.73$  MHz. For the NOT gate, we may modulate  $\alpha'_1 \simeq 1.4347$ , and thus  $\lambda'_1 \simeq 2\pi \times 10.61$  MHz in this case. The decay rate of the resonator  $\kappa$ , the relaxation and dephasing rates of transmon,  $\gamma$  and  $\gamma_\phi$ , are all on the order of kilohertz [35]. For the demonstration purpose, we set  $\kappa = \gamma = \gamma_\phi = 2\pi \times 10$  kHz. Assume that the logical qubit is initially prepared in states of  $|0\rangle_L$  and  $|1\rangle_L$  for the Hadamard and NOT gates, the numerical simulation is presented in Fig. 2(a) and Fig. 2(b), respectively, where high fidelities of 99.85% and 99.96% can be obtained. In our simulation, we have included Hamiltonian in Eq. (5), and thus the obtained high fidelity also verifies our treatment.

At this stage, we turn to the implementation of the holonomic nontrivial two-qubit gates. For this purpose, we only need resonate interaction among the three TLRs from the two logical qubits, i.e., TLR 2 from logical qubit 1 and TLRs 3 and 4 from logical qubit 2. For two logical qubit system, there will exist a six-dimensional DFS

$$\begin{aligned} S_2 = & \{|100100\rangle, |100001\rangle, |001100\rangle, \\ & |001001\rangle, |101000\rangle, |000101\rangle\} \\ \equiv & |00\rangle_L, |01\rangle_L, |10\rangle_L, |11\rangle_L, |00\rangle_L, |E_1\rangle_L, |E_2\rangle_L, \end{aligned} \quad (10)$$

where the former and latter three physical qubits encode the first and second logical qubits, respectively. Then we can encode the logical qubit states same as that of the single-qubit case. To obtain the nontrivial two-qubit gates, we need to induce the interaction within two TLR pairs, i.e., TLRs 2 and 3 and TLRs 2 and 4, connected by blue bonds as shown in Fig. 1a. The wanted interaction can be implemented with three TLRs commonly grounded by a SQUID at their ends as depicted in Fig. 1b. The grounding SQUID is used to establish the localized photonic modes as well as the inter-mode coupling in this coupled circuit. It is noted that the effective inductance of the grounding SQUID here is much smaller than those of the TLRs, then the grounding SQUID can be regarded as a low-voltage shortcut for the three TLRs, and it is this boundary condition that allows the definition of individual TLR modes [36]. Meanwhile, the effective interaction among TLRs can be implemented by dynamic modulation of the Josephson coupling energy of the grounding SQUID via an external two frequencies ac magnetic flux  $\Phi_{ac} = \Phi_{dc} + \sum_{m=1}^2 \Phi_m \cos(\omega_m t + \varphi_m)$ , where  $\Phi_m$ ,  $\omega_m$  and  $\varphi_m$  denote the amplitudes, the fre-

quencies and the initial phases of the modulation, respectively. When  $\Phi_m \ll \Phi_{dc}$ , the resonant coupling Hamiltonian among the three TLRs in the rotating frame reads [36–39]

$$H_{\text{coup}} = \eta_1 a_2^\dagger a_3 e^{i\varphi_1} + \eta_2 a_2^\dagger a_4 e^{i\varphi_2} + \text{H.c.}, \quad (11)$$

where we have assumed that  $\omega_1 = |\omega_{c,2} - \omega_{c,3}|$ ,  $\omega_2 = |\omega_{c,2} - \omega_{c,4}|$ ;  $\eta_m \propto \Phi_m$  and thus can be tuned via the external modulation. Here, we use different frequencies to mediate the two pair interactions, and thus they can be controlled individually. Meanwhile, to avoid possible cross-talk, the two frequencies are largely apart from each other. In our case, we may choose  $\omega_1 = \Delta$  and  $\omega_2 = 2\Delta$ . Therefore, the parameters for the second logical qubit are  $\omega_{c,4} = 7.25$  GHz,  $\omega_{c,3} = 7$  GHz, and  $\omega_{c,2} = 6.5$  GHz. With these parameters, the single-qubit gate parameters for the logical qubit 2 will be the same as the first one. To scale up our proposal, the parameters of the odd and even logical qubits can be chosen to be the same as the first and second logical qubits, respectively.

In our chosen subspace  $S_2$ , the Hamiltonian in Eq. (11) reduces to

$$H_2 = \lambda_2 \left[ \sin \frac{\vartheta}{2} e^{i\varphi} (|E_1\rangle_L \langle 00| + |11\rangle_L \langle E_2|) - \cos \frac{\vartheta}{2} (|E_1\rangle_L \langle 01| + |10\rangle_L \langle E_2|) \right] + \text{H.c.}, \quad (12)$$

where  $\lambda_2 = \sqrt{\eta_1^2 + \eta_2^2}$  is the effective Rabi frequency,  $\tan(\vartheta/2) = \eta_1/\eta_2$ , and  $\varphi = \varphi_1 - \varphi_2 - \pi$ , which all can be tuned via the external modulation. Obviously, the effective Hamiltonian of the total system in the DFS  $S_2$  can be decomposed to two commuting parts as  $H_2 = \lambda_2(H_a + H_b)$  with

$$H_a = \sin \frac{\vartheta}{2} e^{i\varphi} |E_1\rangle_L \langle 00| - \cos \frac{\vartheta}{2} |E_1\rangle_L \langle 01| + \text{H.c.},$$

$$H_b = \sin \frac{\vartheta}{2} e^{-i\varphi} |E_2\rangle_L \langle 11| - \cos \frac{\vartheta}{2} |E_2\rangle_L \langle 10| + \text{H.c.} \quad (13)$$

It is noted that both  $H_a$  and  $H_b$  are similar to Eq. (6), which act nontrivially on the computational subspace  $\{|00\rangle_L, |01\rangle_L\}$  and  $\{|10\rangle_L, |11\rangle_L\}$ , respectively. Therefore, the holonomic two-qubit logical gate can be obtained as

$$U_2 = \begin{pmatrix} \cos \vartheta & \sin \vartheta e^{-i\varphi} & 0 & 0 \\ \sin \vartheta e^{i\varphi} & -\cos \vartheta & 0 & 0 \\ 0 & 0 & -\cos \vartheta & \sin \vartheta e^{-i\varphi} \\ 0 & 0 & \sin \vartheta e^{i\varphi} & \cos \vartheta \end{pmatrix}, \quad (14)$$

which can be varied by controlling  $\vartheta$  and  $\varphi$  via the external modulation.

We further verify the performance of the two-qubit gates. Take  $U_2(\pi/4, 0)$  as an example, when  $\eta_2 = 2\pi \times 10$  MHz,  $\eta_1 = 2\pi \times 4.14$  MHz,  $\eta_1/\eta_2 \simeq \tan(\pi/8)$  in this

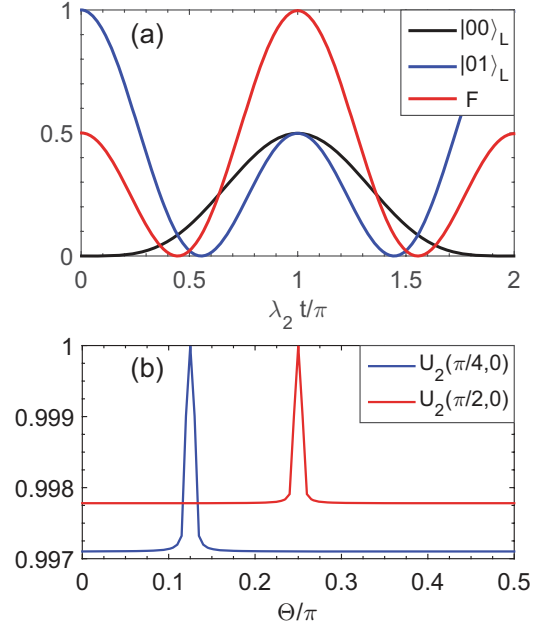


FIG. 3. (a) Qubit state populations and fidelity under two-qubit operator  $U_2(\pi/4, 0)$  with initial state  $|01\rangle_L$ . (b) Maximum fidelity as the function of  $\Theta$  in unit of  $\pi$  with blue and red line under gate operation  $U_2(\pi/4, 0)$  and  $U_2(\pi/2, 0)$ , respectively.

case, and thus  $\lambda_2 = 14.14$  MHz. For the initial state  $|01\rangle$ , as shown in Fig. 3(a), we obtain a high fidelity of 99.71% for the two-qubit gate, which is comparable to the single qubit case. This is sharp contrast with previous implementations, where two-qubit gate usually induced by large detuning, and thus effective interaction strength will be much small than the single-qubit case. In our scheme, due to fact that all the interactions used here are resonant, and thus the  $\lambda_2$  is still on the same order as that of in the single-qubit case. In addition, in order to discover the influence from the different initial state, as shown in Fig. 3(b), we have investigated different cases by choosing different  $\Theta$  in the initial state of  $|\psi\rangle = \cos \Theta |00\rangle_L + \sin \Theta |01\rangle_L$  under operations  $U_2(\pi/4, 0)$  and  $U_2(\pi/2, 0)$  respectively.

In summary, we have proposed to implement a universal set of non-adiabatic holonomic quantum gates in DFS with the typical circuit QED lattice. By controlling the amplitude and relative phase of the driving lasers, we can realize arbitrary single-qubit and two-qubit gates through resonate interactions. Numerical simulation shows that our scheme is stable to the deviation of corresponding experimental parameters and insensitive to decoherence. Therefore, our scheme presents a promising way of implementation high fidelity HQC.

This work is supported by the NFRPC (No. 2013CB921804), the NSFC (No. 11374117), the PCSIRT (No. IRT1243), the Education Department of Anhui

Province (No. KJ2015A299), and NJU (No. M28015).

\* zyxue@scnu.edu.cn

† jianzhou8627@163.com

‡ huyong@mail.hust.edu.cn

- [1] M. V. Berry, Proc. R. Soc. Lond. A **392**, 45 (1984).
- [2] Y. Aharonov and J. Anandan, Phys. Rev. Lett. **58**, 1593 (1987).
- [3] F. Wilczek and A. Zee, Phys. Rev. Lett. **52**, 2111 (1984).
- [4] J. Anandan, Phys. Lett. A **133**, 171–175 (1988).
- [5] P. Zanardi and M. Rasetti, Phys. Lett. A **264**, 94–99 (1999).
- [6] L.-M. Duan, J. I. Cirac, and P. Zoller, Science **292**, 1695–1697 (2001).
- [7] A. Recati, T. Calarco, P. Zanardi, J. I. Cirac, and P. Zoller, Phys. Rev. A **66**, 032309 (2002).
- [8] L. Faoro, J. Siewert, and R. Fazio, Phys. Rev. Lett. **90**, 028301 (2003).
- [9] P. Zhang, Z. D. Wang, J. D. Sun, and C. P. Sun, Phys. Rev. A **71**, 042301 (2005).
- [10] I. Kamleitner, P. Solinas, C. Müller, A. Shnirman, and M. Möttönen, Phys. Rev. B **83**, 214518 (2011).
- [11] V. V. Albert, S. Krastanov, C. Shen, R.-B. Liu, R. J. Schoelkopf, M. Mirrahimi, M. H. Devoret, and L. Jiang, arXiv:1503.00194.
- [12] Wang Xiang-Bin and M. Keiji, Phys. Rev. Lett. **87**, 097901 (2001).
- [13] S.-L. Zhu and Z. D. Wang, Phys. Rev. Lett. **89**, 097902 (2002).
- [14] E. Sjöqvist, D. M. Tong, L. Mauritz Andersson, B. Hessmo, M. Johansson, and K. Singh, New J. Phys. **14**, 103035 (2012).
- [15] G. Feng, G. Xu, and G. Long, Phys. Rev. Lett. **110**, 190501 (2013).
- [16] A. A. Abdumalikov, J. M. Fink, K. Juliusson, M. Pechal, S. Berger, A. Wallraff, and S. Filipp, Nature **496**, 482–485 (2013).
- [17] C. Zu, W.-B. Wang, L. He, W.-G. Zhang, C.-Y. Dai, F. Wang, and L.-M. Duan, Nature **514**, 72–75 (2014).
- [18] S. Arroyo-Camejo, A. Lazarev, S. W. Hell, and G. Balasubramanian, Nat. Commun. **5**, 4870 (2014).
- [19] L.-A. Wu, P. Zanardi, and D. A. Lidar, Phys. Rev. Lett. **95**, 130501 (2005).
- [20] G. F. Xu, J. Zhang, D. M. Tong, E. Sjöqvist, and L. C. Kwek, Phys. Rev. Lett. **109**, 170501 (2012).
- [21] Z.-T. Liang, Y.-X. Du, W. Huang, Z.-Y. Xue, and H. Yan, Phys. Rev. A **89**, 062312 (2014).
- [22] J. Zhang, L.-C. Kwek, E. Sjöqvist, D. M. Tong, and P. Zanardi, Phys. Rev. A **89**, 042302 (2014).
- [23] G.-F. Xu and G.-L. Long, Sci. Rep. **4**, 6814 (2014).
- [24] Z.-Y. Xue, J. Zhou, and Z. D. Wang, Phys. Rev. A **92**, 022320 (2015).
- [25] J. Zhou, W.-C. Yu, Y.-M. Gao, and Z.-Y. Xue, Opt. Express **23**, 14027–14035 (2015).
- [26] M. J. Peterer, S. J. Bader, X. Jin, F. Yan, A. Kamal, T. J. Gudmundsen, P. J. Leek, T. P. Orlando, W. D. Oliver, and S. Gustavsson, Phys. Rev. Lett. **114**, 010501 (2015).
- [27] L.-M. Duan and G.-C. Guo, Phys. Rev. Lett. **79**, 1953 (1997).
- [28] P. Zanardi and M. Rasetti, Phys. Rev. Lett. **79**, 3306 (1997).
- [29] D. A. Lidar, I. L. Chuang, and K. B. Whaley, Phys. Rev. Lett. **81**, 2594 (1998).
- [30] L. Steffen, Y. Salathe, M. Oppliger, P. Kurpiers, M. Baur, C. Lang, C. Eichler, G. Puebla-Hellmann, A. Fedorov, and A. Wallraff, Nature **500**, 319–22 (2013).
- [31] J. D. Strand, M. Ware, F. Beaudoin, T. A. Ohki, B. R. Johnson, A. Blais, and B. L. T. Plourde, Phys. Rev. B **87**, 220505 (2013).
- [32] J. M. Fink, R. Bianchetti, M. Baur, M. Göppl, L. Steffen, S. Filipp, P. J. Leek, A. Blais, and A. Wallraff, Phys. Rev. Lett. **103**, 083601 (2009).
- [33] G. Lindblad, Commun. Math. Phys. **48**, 119–130 (1976).
- [34] A. Baust, E. Hoffmann, M. Haerberlein, M. J. Schwarz, P. Eder, J. Goetz, F. Wulschner, E. Xie, L. Zhong, F. Quijandría, B. Peropadre, D. Zueco, J.-J. García Ripoll, E. Solano, K. Fedorov, E. P. Menzel, F. Deppe, A. Marx, and R. Gross, Phys. Rev. B **91**, 014515 (2015).
- [35] M. H. Devoret and R. J. Schoelkopf, Science **339**, 1169 (2013).
- [36] S. Felicetti, M. Sanz, L. Lamata, G. Romero, G. Johansson, P. Delsing, and E. Solano, Phys. Rev. Lett. **113**, 093602 (2014).
- [37] Y.-P. Wang, W. Wang, Z.-Y. Xue, W.-L. Yang, Y. Hu, and Y. Wu, Sci. Rep. **5**, 8352 (2015).
- [38] Y.-P. Wang, W.-L. Yang, Z.-Y. Xue, Y. Hu, and Y. Wu, arXiv:1506.01279 (2015).
- [39] F. Wulschner, J. Goetz, F. R. Koessel, E. Hoffmann, A. Baust, P. Eder, M. Fischer, M. Haerberlein, M. J. Schwarz, M. Pernpeintner, E. Xie, L. Zhong, C. W. Zollitsch, B. Peropadre, J.-J. Garcia Ripoll, E. Solano, K. Fedorov, E. P. Menzel, F. Deppe, A. Marx, and R. Gross, arXiv:1508.06758 (2015).